Analysis of ground motion caused by propagating air pressure waves

H. Werkle and G. Waas

Hochtief A.G., Abt. KTI, Bockenheimer Landstr. 24, 6000 Frankfurt/Main 1, West Germany

The soil is assumed to be a horizontally layered viscoelastic medium over a rigid base. A semi-analytical method is used to calculate the Green functions for line loads in the frequency domain. The displacements in the soil are then obtained by spatial convolution and Fourier transforms from the frequency to the time domain. The influence of significant parameters is studied for a homogeneous layer. Maximum response is obtained when the air pressure wave velocity equals the Rayleigh wave velocity in the soil. The response spectra computed for an actual soil profile, which is subjected to an air pressure wave from a deflagration-type explosion, show predominant response at frequencies, which are significantly higher than those of earthquake motion.

1. INTRODUCTION

In most problems of soil dynamics loads vary in time but do not change their spatial position. A problem in which the spatial motion of the load is important, is that of an air pressure wave which results from the explosion of a gas cloud and propagates over the surface of the ground. A similar loading is produced by sonic booms. In the following, ground vibrations caused by propagating air pressure waves are investigated. They are of interest in the design of underground and surface structures with high safety requirements.

A simple analysis approach to the problem of a moving air pressure load is based on the assumption of one-dimensional wave propagation in soil[1]. Spatial wave reflections and refractions at soil layer interfaces as well as the generation of surface waves are neglected. In more sophisticated analyses the soil has been considered as an elastic half-space. An early solution for arbitrarily moving loads on a half-space under plane strain conditions was obtained through a Fourier transform by Sneddon[2] in form of an integral. Cinelli and Fugelso[3] evaluated this integral for the case of a moving load which consists of a sudden rise and an exponential decay. They also derived integral solutions for the corresponding axisymmetric case. Cole and Huth[4] have presented formulae and graphs for line loads moving on an elastic half-space. Results for a line load of finite length have been given by Baron *et al.*[5]. In all these studies it was assumed that the load travels with constant velocity, so that a steady displacement pattern appears with respect to an observer who moves along with the load. Formal solutions for axisymmetric and point loads moving with variable velocity have been derived by Miles[6] and Payton[7], respectively. The results are given as integrals which require a numerical solution.

With the development of powerful computers, purely numerical methods have become attractive. They make it possible to simulate more closely the actual site conditions and nonlinear soil behavior. Analyses for plane and axisymmetric air pressure loads on a layered soil with nonlinear behaviour have been carried out by Rischbieter[8] using a finite difference method. Nelson has studied the response of a structure caused by a moving air pressure load employing a finite element method[9–11]. However, the analyses of two-dimensional problems by purely numerical methods requires a large number of elements and therefore a major computational effort.

In order to reduce the numerical effort, a semi-analytical method is used in the present study. A deflagration-type air pressure load with a constant peak amplitude and a plane wave front is considered. The soil is assumed to be a layered viscoelastic medium over a rigid base. Results are presented for the case of a homogeneous soil layer in dimensionless form and the response of an actual site with layered soil is studied.

2. METHOD OF ANALYSIS

The computation of the soil motion is based on a line load solution (Green function) in the frequency domain. Its derivation is outlined first. Then the displacements caused by a moving air pressure wave are computed by spatial convolution of the Green function and the load distribution. Finally, the time history response is obtained by a Fourier transform. The transform requires only a small computational effort if the load time-history is independent of the space variable except for a phase shift and a scaling function.

Any time-dependent function $f(t)$ (satisfying certain conditions[16]) with a finite period T can be transformed into the frequency domain:

$$F_s = \frac{1}{T}\int_0^T f(t)\cdot e^{-i\omega_s t}\,dt; \qquad \omega_s = \frac{2\pi}{T}\cdot s \qquad (1a)$$

Accepted July 1986. Discussion closes December 1987.

0267-7261/87/040194-09$2.00

and

$$f(t)=\sum_{-\infty}^{\infty} F_s \cdot e^{i\omega_s t} \qquad s=\ldots -2,-1,0,1,2,\ldots \tag{1b}$$

In the following, all variables for displacements and loads refer to the frequency domain.

The motion in a medium under plane strain conditions may be expressed by

$$\begin{Bmatrix} u(x,z) \\ w(x,z) \end{Bmatrix} = \sum_j \alpha_j \cdot \begin{Bmatrix} X_j(z) \\ Z_j(z) \end{Bmatrix} \cdot e^{-i\cdot k_j x} \tag{2}$$

where u and w denote the displacements in the horizontal x- and vertical z-direction, respectively. For a load $p(x)$ (e.g., at $z=0$), the functions $X_j(z)$ and $Z_j(z)$ might be obtained by a spatial Fourier transform from the x-domain into the k_j-domain[2]. Equation (2) then defines the discrete inverse Fourier transformation into the x-domain. If the problem of freely propagating waves in the layered medium over a fixed base is considered (i.e., no external loads act on the medium), $X_j(z)$, $Z_j(z)$ and k_j are obtained as solution of an eigenvalue problem[14]. The summation in equation (2) denotes the superposition of the eigenvectors which are multiplied by participation factors. The participation factors can be determined from boundary conditions for stresses or displacements at a vertical line, e.g., at $x=0$. The method is called semi-analytic as it uses approximate solutions in the vertical direction and analytical solutions in the horizontal direction (see appendix). It is employed in this study.

For a vertical line load p, acting at $x=x_l$ on the surface of the layered medium, Fig. 1, the horizontal and vertical displacements $\underline{u}$ and $\underline{w}$ of the layer interfaces at $x=x_m$ are:

$$\underline{\tilde{u}}=\underline{g}(x_m-x_l)\cdot p; \qquad \underline{\tilde{u}}=\begin{Bmatrix} \underline{u} \\ \underline{w} \end{Bmatrix} \tag{3}$$

in which

$$\underline{g}(x_m-x_l)=-\frac{1}{2}\cdot\sum_{j=1}^{2n_z} k_j \cdot Z_{oj}\cdot \xi_j \cdot \begin{Bmatrix} \operatorname{sign}(x_m-x_l)\cdot \underline{X}_j \\ i\cdot \underline{Z}_j \end{Bmatrix} \tag{3a}$$

and

$$\xi_j = e^{-i\cdot k_j\cdot|x_m-x_l|} \tag{3b}$$

Z_{oj} = element of $\underline{Z}_j$ refering to the soil surface ($z=0$).

The vectors $\underline{X}_j$, $\underline{Z}_j$ and the parameters k_j are obtained

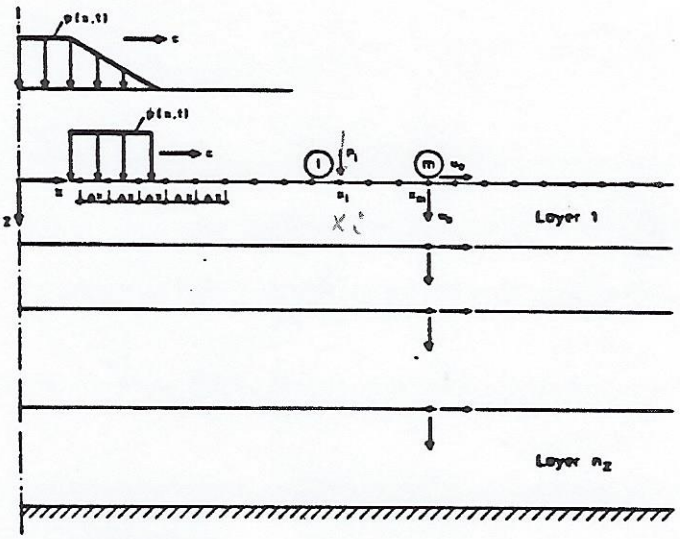

Fig. 1. Soil model

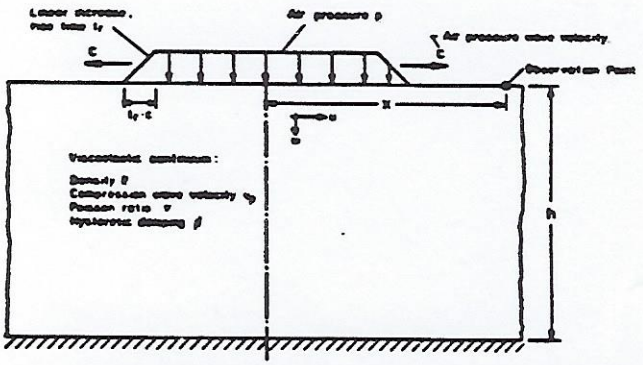

Fig. 2. Propagating air pressure wave on a viscoelastic layer

Table 1. Fourier transformation of air pressure rate time-histories

Pressure p	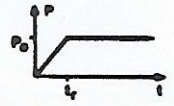	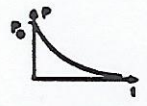
Pressure rate $\dot{p}$	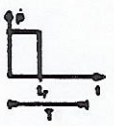	
Fourier coefficients of the pressure rate	$\dot{p}_s=\frac{p_0}{T}$ for $s=0$ $=\frac{p_0}{T}\cdot\frac{i}{\omega_s\cdot t_r}(e^{-i\omega_s t_r}-1)$ for $s\neq 0$	$\dot{p}_s=\frac{p_0}{T\cdot(1+i\omega_s/\gamma)}(e^{-\gamma\cdot T}-1)$

from the solution of the eigenvalue problem[13,14]. $\underline{X}_j$ and $\underline{Z}_j$ denote the horizontal and vertical displacement, respectively, and k_j the corresponding eigenvalue in the jth mode. The elements of the vectors refer to the layer interfaces, where in each layer a linear variation of the displacements over the height is assumed. The normalization of the eigenvectors is understood as in Refs 13 and 14. The summation is performed over 2^*n_z modes, where n_z is the number of layers.

Instead of a line load, a uniform strip load $\bar{p}=p/\Delta x$ from $x=x_l-\Delta x/2$ to $x=x_l+\Delta x/2$ may be considered. Integration of equations (3a,b) yields in this case with $\kappa=k_j\cdot\Delta x/2$

$$\xi_j=\frac{\sin\kappa}{\kappa}\cdot e^{-ik_j|x_m-x_l|}\approx\left(1-\frac{\kappa^2}{6}\right)\cdot e^{-ik_j|x_m-x_l|}$$

$$\text{for } m\neq l \tag{4a}$$

and

$$\xi_j=\frac{i}{\kappa}\cdot(e^{-i\kappa}-1)\approx\left(1-\frac{i}{2}\kappa\right)\qquad\text{for } m=l \tag{4b}$$

Equations (3) (with $\bar{\bar{p}}=\bar{p}\cdot\Delta x$) and (3a) remain valid.

For loads applied throughout the x-domain, the displacements at $x=x_m$ are given by the spatial convolution integral

$$\underline{\tilde{u}}(x_m)=\int_{-\infty}^{\infty}\underline{g}(x_m-x)\cdot\bar{p}(x)\cdot\mathrm{d}x \tag{5}$$

The discretized finite form of equation (5) for n_x equal intervals Δx is[16]:

$$\underline{\tilde{u}}(m\cdot\Delta x)=\sum_{l=0}^{n_x-1}\underline{g}((m-l)\cdot\Delta x)\cdot p(l\cdot\Delta x) \tag{6}$$

The Fourier transformation of the pressure time-history into the frequency domain would generally be performed for each coordinate $x_l=l^*\Delta x$. However, if the time-histories at different coordinates x_l are similar, i.e., they differ only by a phase lag $t_a(x_l)$ and by an amplification function $\alpha(x_l)$, the transformation needs to be performed only for one location. Letting $p(0)$ denote the Fourier transform of the pressure time history at $x=0$, the transform at $x=x_l$ is

$$p(x_l)=\alpha(x_l)\cdot p(0)\cdot e^{-i\omega_n t_a(x_l)} \tag{7}$$

Further computational savings are possible for constant propagation velocity c. Then the lag time is $t_a(x_l)=l\cdot\Delta x/c$, and the evaluation of the exponential function in equation (7) can be reduced to repeated multiplications

$$e^{-i\omega_n t_a(x_l)}=(e^{-i\omega_n\Delta x/c})^l \tag{8}$$

The Fourier transformation of the load time-histories are performed over a finite period T for a finite number of points n_x. As the finite transform implies periodic loading the period T should be large enough to allow for attenuation of the response at the observation points and to let the air pressure wave sweep across the discretized x-region. The latter conditions leads for constant c to $T\geqslant n_x\cdot\Delta x/c$.

The spatial discretization is extended to a large enough distance from the observation points so that a compression wave (P-wave) generated at the spatial break-off-point does not reach the observation points during the time of interest.

The number of time steps n_t and hence the highest frequency $f=n_t/(2^*T)$ considered in the analysis should be large enough to represent the air pressure time-history by the Fourier series with sufficient accuracy.

In the present application it is convenient to use the time rates rather than the basic variables in equations (5) and (6); i.e., the particle velocities $\dot{u},\dot{w}$ and the loading rate $\dot{p}$ instead of the displacements u,w and the loading p, repectively. For two typical time-histories the Fourier transformations of the loading rates are given in Table 1. The first load function is representative for a deflagration; the second corresponds to a detonation.

3. HOMOGENEOUS LAYER

The motion of a homogeneous viscoelastic soil layer subjected to a deflagration-type air pressure wave is studied. At any point on the surface, the air pressure rises linearly from zero to p during the rise time t_r after the arrival of the air pressure wave, and remains constant thereafter. The slow decrease of the pressure after the maximum load in actual deflagrations is not considered here, since it affects only the low frequency content and hardly influences peak velocities and peak accelerations of the soil motion. The air pressure wave propagates simultaneously in the positive and negative x-direction, see Fig. 2.

The motion of the layer depends on the dimensionless parameters

c/v_p — ratio of the air pressure propagation velocity c to the P-wave velocity $v_p=\sqrt{(\lambda+2G)/\rho}$ with λ = Lame-constant, G = shear modulus and ρ = density

$\tau_r=\dfrac{v_p\cdot t_r}{h}$ — ratio of the load rise time to the travel time of a P-wave over the height h

$\nu=\dfrac{\lambda}{2\cdot(\lambda+G)}$ — Poisson ratio

β — hysteretic damping ratio

In the example, $\nu=0.3$ and $\beta=0.05$. The total height h of the layer is discretized into 25 sublayers ($5^*0.025h$, $10^*0.0375h$, $10^*0.05h$, from top to bottom). In the horizontal direction the ground surface is discretized using intervals of $\Delta x=0.05^*h$. The time-history is described by 256 time steps $\Delta t=0.39^*h/v$.

The ground motion is presented in Figs 3 to 8 in terms of dimensionless displacements, velocities and accelerations. The scaling factors are

$$w_0=\frac{p_0\cdot h}{\lambda+2G} \tag{9a}$$

$$v_H=\frac{p_0}{\rho\cdot v_p} \tag{9b}$$

$$a_H=\frac{p_0}{t_r\cdot\rho\cdot v_p} \tag{9c}$$

respectively. The value w_0 represents the displacement of

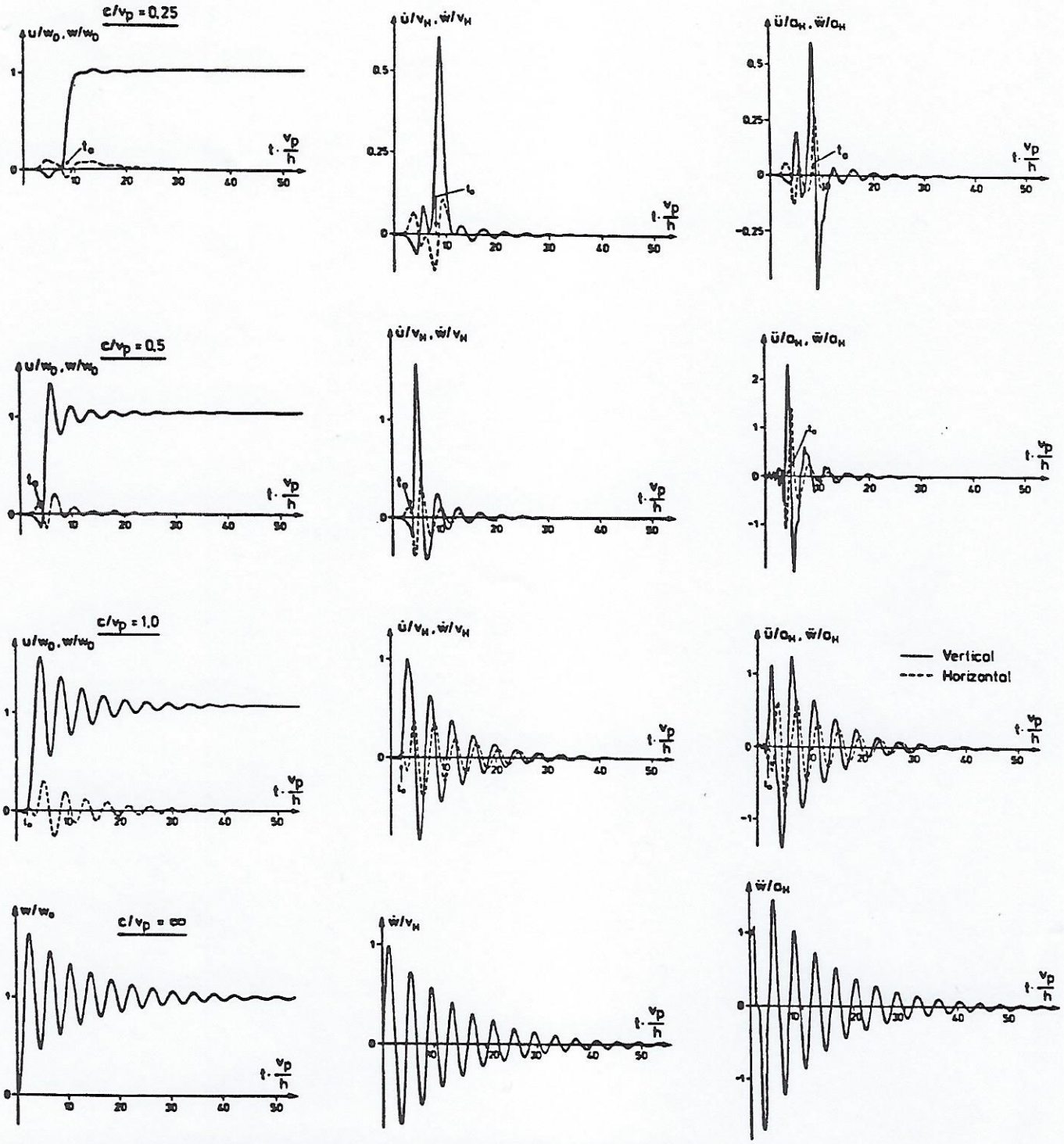

Fig. 3. Particle motions for different air pressure wave velocities, z=0, x/h=2.0, τ_r=1.0

a homogeneous layer under a static uniform load p_0; v_H and a_H are the maximum velocity and acceleration, respectively, in a homogeneous halfspace loaded by a uniform pressure which rises linearly during the time t_r from zero to p_0.

The time-histories of the motions at the soil surface are shown in Fig. 3 for different wave velocity ratios c/v_p. They refer to a line $x=2*h$ and the rise time ratio $\tau_r=1$.

For low air pressure wave velocities ($c/v_p=0.25$) considerable motion occurs before the air pressure wave arrives, because the surface waves in the ground propagate faster than the air pressure wave. The acceleration time history is characterized by a high frequency content and few significant peaks. This result is qualitatively confirmed by measurements of ground vibrations during test explosions near the centre of explosion[18].

For the ratio $c/v_p=0.5$ the air pressure wave velocity nearly equals the Rayleigh wave velocity in the soil (– in an elastic half-space with $\nu=0.3$ the Rayleigh wave velocity is $v_R\approx 0.5v_p$)[17]. Large amplitudes occur only after the arrival of the air pressure wave. The amplitudes are considerably higher and the time-histories show stronger oscillations than in the case $c/v_p=0.25$.

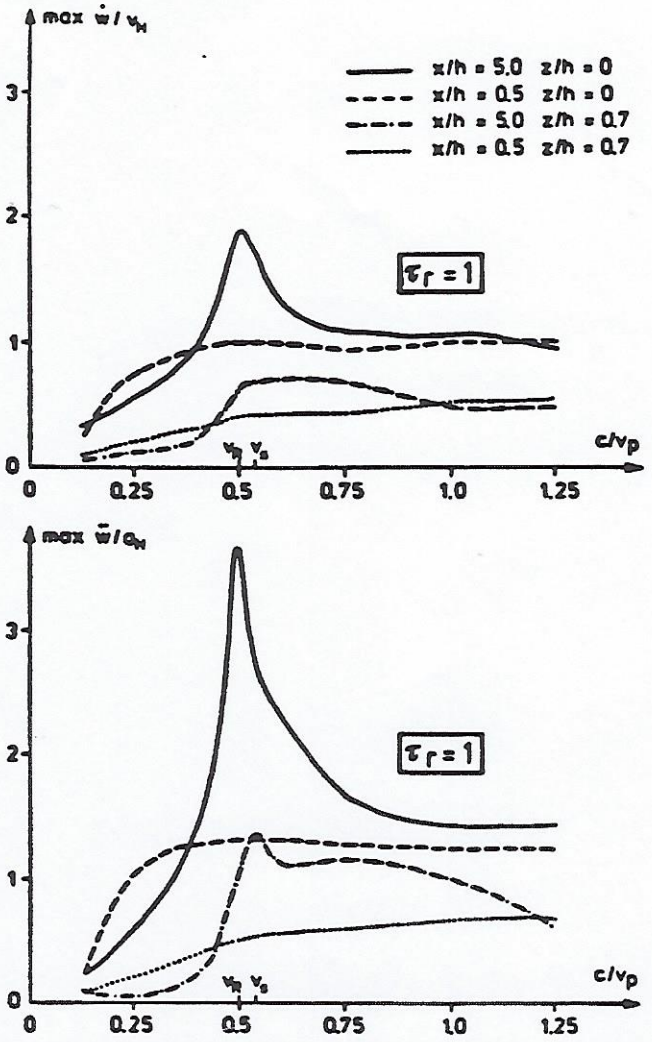

Fig. 4. Vertical peak velocity and acceleration versus the wave velocity ratio c/v_p, $\tau_r = 1.0$, $\beta = 5\%$

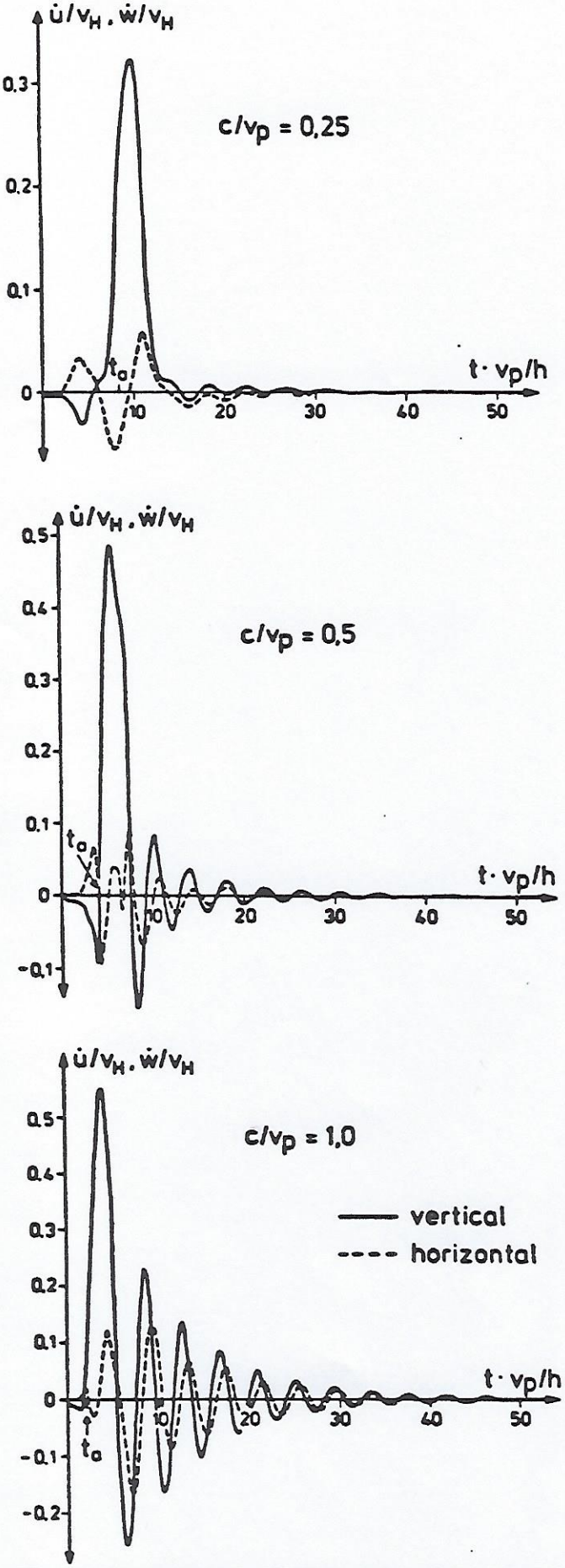

Fig. 5. Particle velocities for loading rate $\tau_r = 3.0$ and different air pressure wave velocities, $z = 0$, $x/h = 2.0$

For high air pressure wave velocities, $c/v_p = 1$, these vibrations are very pronounced. If the air pressure wave velocity is greater than the compression wave velocity in soil, the soil motion cannot start before the arrival of the air pressure wave. The time-histories reveal the dominance of vertically propagating compression waves which are reflected at the rigid base and at the surface and attenuate with time due to material damping. The predominant frequency is the first resonant frequency of the soil layer, i.e., $f = v_p/(4h)$. Thus, the response can be well approximated by one-dimensional wave propagation theory when the air pressure wave velocity is larger than the compression wave velocity in the ground. For a homogeneous layer on a rigid base one obtains the vertical displacement at the surface in the frequency domain as:

$$w = w_0 \cdot \tan(\bar{\chi})/\bar{\chi} \cdot p/p_0 \qquad (10)$$

with

$$\bar{\chi} = \omega_s \cdot h \cdot \sqrt{\rho/((\lambda + 2G) \cdot (1 + 2\beta i)} \qquad (10a)$$

The velocity of the ground surface motion as computed by the one-dimensional theory ($v_p/c = \infty$) for $\tau_r = 1$ is shown in Fig. 3 vs. time. The time-history is similar to that computed by the two-dimensional theory and peak

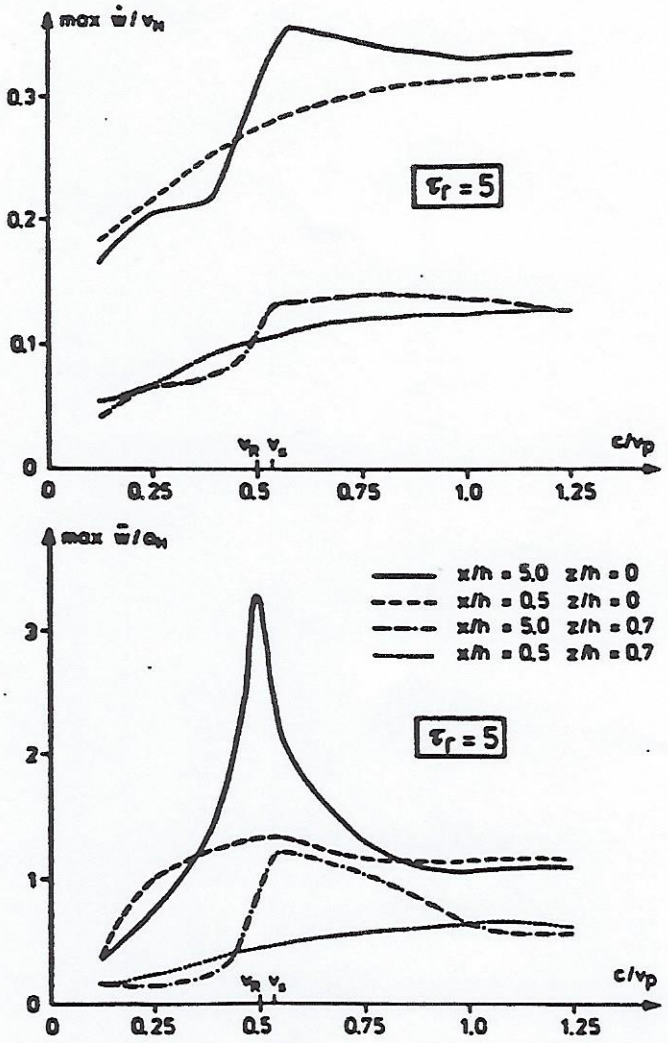

Fig. 6. Vertical peal velocity and acceleration versus the wave velocity ratio c/v_p, $\tau_r = 5.0$, $\beta = 5\%$

response values are approximately the same. The one-dimensional results indicate less damping; there is no radiation damping in this case. The maximum velocity is not larger than the peak value in an elastic half-space subjected to a monotonically increasing load, equation (9b); wave reflections at the layer base reduce the peak velocity.

Fig. 4 shows the effect of c/v_p on the peak values. As long as c is smaller than v_p, the particle velocities increase with c/v_p. When the air pressure wave velocity c equals the Rayleigh wave velocity $v_R = 0.5 \cdot v_p$, the ground motion has a peak. For a soil without internal damping and for $x \to \infty$ the response at $c = v_R$ would tend to infinity.

The ground motion depends also on the load rise time. For a rise time ratio $\tau_r = 3$ particle velocity time-histories are shown in Fig. 5. They are similar to those for $\tau_r = 1$ in Fig. 3, but their amplitudes are considerably less. Peak velocities and accelerations decrease with increasing rise time (compare Figs 4 and 6). The reduction of peak velocity is caused by wave reflection at the rigid base during the load rise time and the reduction of peak acceleration is due to the decreasing loading rate, see scaling factor a_n in equation (8).

The variation of the ground motion with distance from the centre of explosion is demonstrated for a case with low air pressure wave velocity ratio ($c/v_p = 0.25$) in Fig. 7.

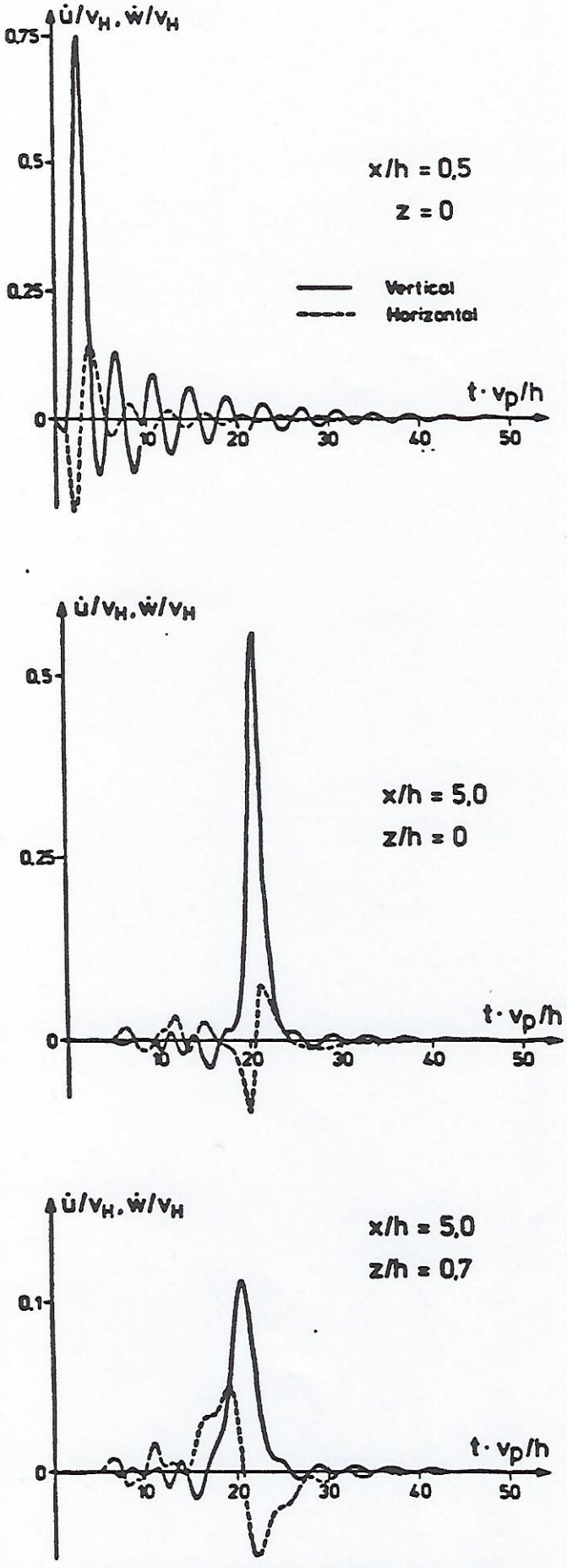

Fig. 7. Particle velocities at different locations, $c/v_p = 0.25$, $\tau_r = 1.0$

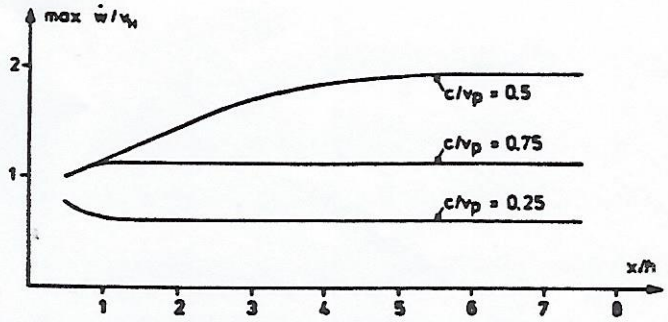

Fig. 8. Maximum vertical particle velocity versus distance from the centre of explosion, $\tau_r = 1.0$

Near the centre of explosion the high velocity peak caused by the rise of the air pressure is followed by oscillations at the resonant frequency of the layer. At greater distance ($x/h = 5$) these oscillations attenuate more rapidly, and the velocity peak is preceded by motions due to ground waves which arrive before the air pressure wave.

The ground waves are generalized Rayleigh waves which consist of interfering *P*- and vertically polarized *S*-waves. Due to the rigid base their velocity varies with frequency. However, at the higher frequencies excited by the pressure pulse, the Rayleigh waves in the layer travel with the velocity of Rayleigh waves in a homogeneous half-space.

Fig. 8 shows that the peak value of the response varies only slightly with distance from the center of explosion for low and high velocity ratios c/v_p. However, for $c/v_p = 0.5$, the peak velocity increases with distance and then levels off to a maximum value. This indicates that Rayleigh waves are excited most effectively when the air pressure wave sweeps across the ground with the Rayleigh wave velocity. The maximum response is limited by the internal damping of the soil.

Within the layer the amplitudes of the soil motion are smaller than at the surface, Fig. 7c.

The response spectrum method is often used to analyse structures subjected to ground motions. Therefore, acceleration response spectra are computed. They are presented in Fig. 9 for two distances from the centre of explosion and for three wave velocity ratios. The horizontal and vertical response accelerations are normalized with respect to equation (9), and are plotted versus the dimensionless frequency $f^* h/v_p$. Pronounced peaks occur at the layer natural frequencies of the soil layer especially near the first frequency for vertically propagating *P*-waves. For $c/v_p = 0.5$ the effect of the Rayleigh waves shows up in the change of the frequency content as well as in the magnification of the response, especially in the horizontal direction. Response spectra at different depths under the soil surface show that the amplitudes decrease with depth. However, the shape of the spectra changes only slightly, Fig. 10. The horizontal component is larger at $z/h = 0.7$ than at $z/h = 0.3$; this is due to the mode shapes of the Rayleigh wave.

4. LAYERED SOIL

An actual soil profile, typical for sediments in a river valley, consisting of sand and gravel is considered next. The shear wave velocity increases from 300 m/s at the surface to 590 m/s at a depth of 80 m (Table 2). The total height of the soil profile of 160 m is discretized in 24 layers, along the soil surface the discretization interval is $x = 2$ m. For the discrete Fourier transform a period of 3 s and 256 time steps are used. The explosion is of deflagration-type; the air pressure wave propagates in the positive and negative x-direction with a constant velocity of 340 m/s. This velocity is near the shear wave velocity in the upper layers.

The time-histories of the particle velocity on the soil

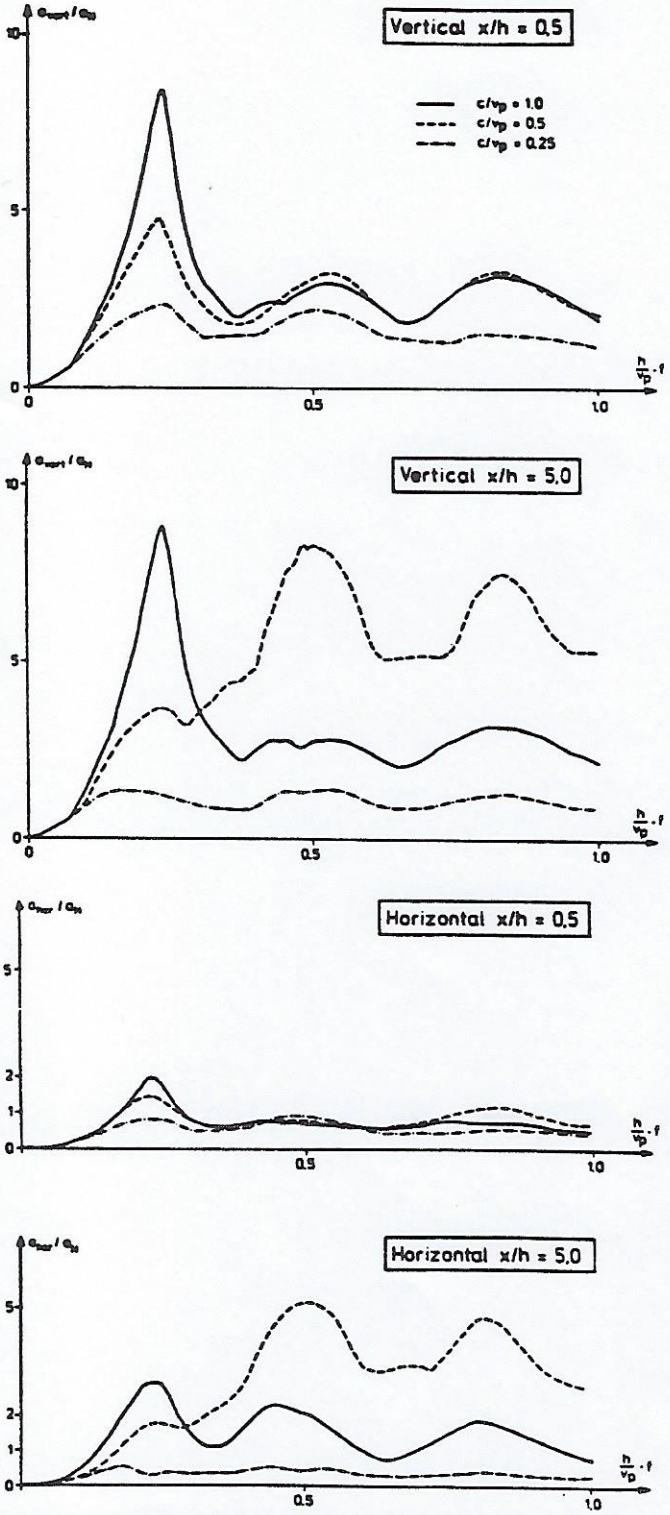

Fig. 9. Acceleration response spectra at the soil surface for 2% damping, $\tau_r = 3.0$

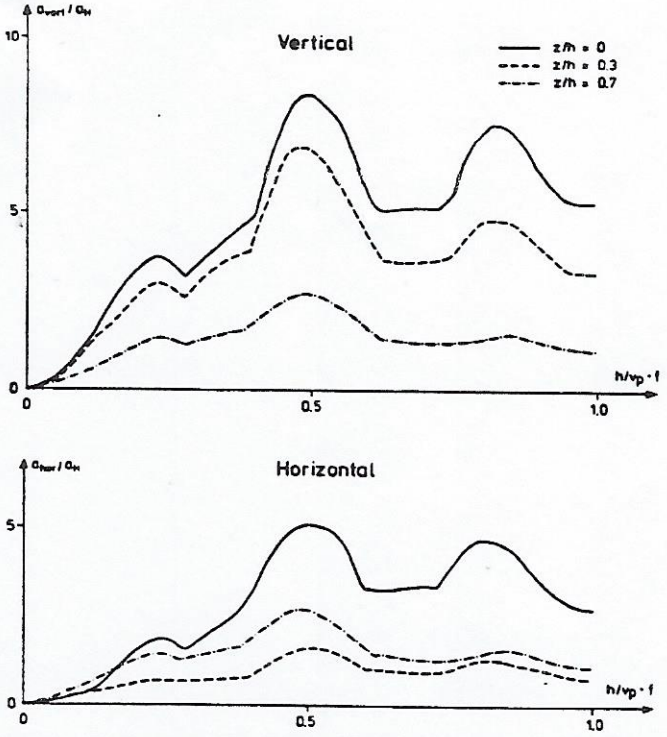

Fig. 10. Acceleration response spectra in different depths, x/h = 5.0, c/v_p = 0.5, τ_r = 3.0

Table 2. Dynamic soil properties for layered soil case

Depth [m]	Mass density [$KS \cdot s^2/m^4$]	Shear modulus [MN/m^2]	Poisson-ratio ν	Hysteretic damping β
0–5	1.60	150	0.30	0.05
5–12	1.90	165	0.48	0.05
12–30	1.95	220	0.48	0.03
30–60	2.00	330	0.47	0.03
60–88	2.05	530	0.46	0.02
88–148	2.10	700	0.45	0.02

surface at the distances of 30 m and 100 m away from the centre of explosion are shown in Fig. 11. They are similar to those in a homogeneous layer at air pressure velocities near the Rayleigh wave velocity in the soil. The vertical and horizontal acceleration response spectra for 5% damping at different distances from the centre of explosion are given in Fig. 12. The motion increases with the distance from the centre of explosion due to surface waves in the layered soil. The peak values in the response spectra are at high frequencies. It should be noted that for large stiff structures these frequencies may be filtered out by kinematic and inertial soil structure interaction.

5. CONCLUSIONS

Propagating air pressure waves caused by gas cloud explosions of deflagration type produce ground accelerations with a high frequency content and only a few significant cycles. The response depends on the ratio of the air pressure wave velocity c and Rayleigh wave velocity v_R in soil. Maximum response is obtained for $c = v_R$. In this case two-dimensional wave propagation effects and material damping of the soil are very important. For $c > v_R$ simplified one-dimensional methods which consider only vertically propagating P-waves in soil may be used. The acceleration response spectra of ground motions caused by gas cloud explosions may be of similar magnitude as those of earthquakes, but their dominant frequencies are much higher.

7. ACKNOWLEDGEMENTS

The authors wish to express their thanks for the financial support received from the Bundesminister für Forschung und Technologie (Contract No. 150416) and the assistance of the Gesellschaft für Reaktorsicherheit (GRS), Köln, Germany.

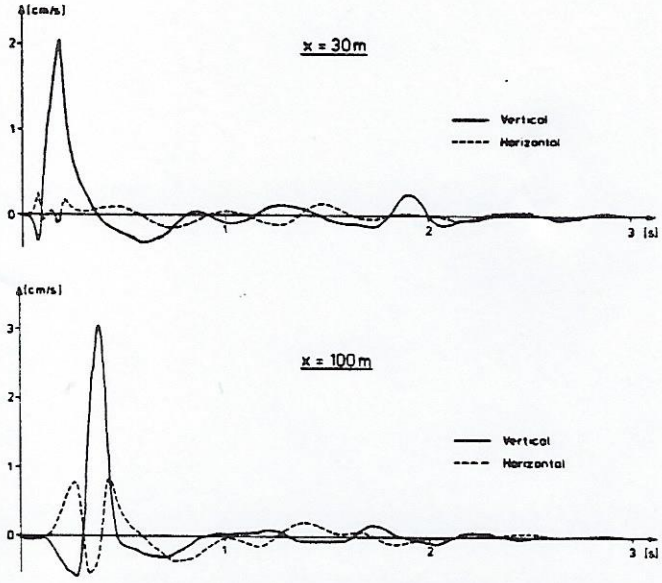

Fig. 11. Particle velocity at the surface of a layered soil

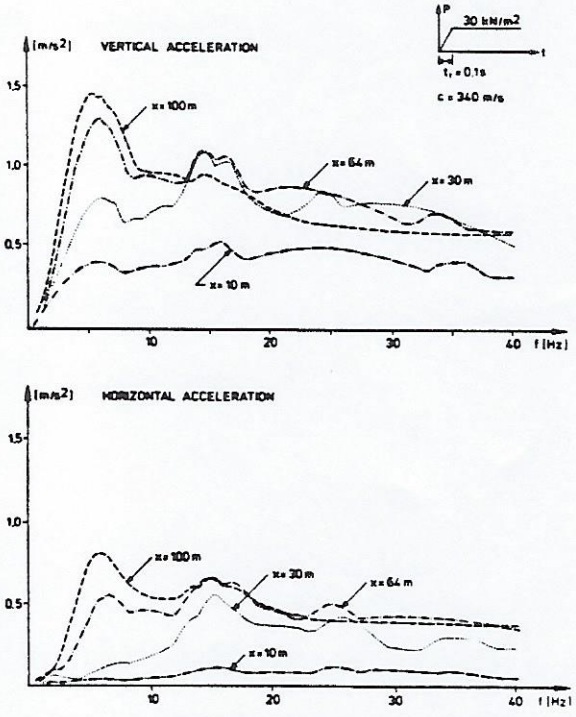

Fig. 12. Acceleration response spectra on the surface of a layered soil

REFERENCES

1 Wu, Tien Hsing, Soil dynamics, Allyn and Bacon Inc., Boston, 1971
2 Sneddon, I. N. Fourier transforms, McGraw Hill, New York, 1951
3 Cinelli, G. and Fugelso, L. E. Theoretical study of ground motion produced by nuclear blasts, Techn. Doc. Report AFSWC-TR-80, Air Force Special Weapon Center, 1959
4 Cole, J. and Huth, J. Stresses produced in a half plane by moving loads, *Transactions ASME, J. Appl. Mech.*, 1958
5 Baron, M. L., Bleich, H. H. and Wright, J. P. Ground shock due to Rayleigh waves from sonic booms, Proc. American Soc. Civ. Engineers, EM5, 1967
6 Miles, J. W. On the response of an elastic halfspace to a moving blast wave, Transactions ASME, *J. Appl. Mech.*, 1960
7 Payton, R. G. An application of the dynamic Betti-Rayleigh reciprical theorem to moving point loads in elastic media, *Quarterly of Appl. Mathematics*, 1964, 21
8 Rischbieter, F. and Michelmann, K. Bodenwelle bei Gasexplosionen, Beitrag der induzierten Bodenwelle zur Belastung von KKW-Strukturen, Batelle-Institut, Frankfurt, 1984
9 Nelson, I. Numerical solution of problems involving loading, Proc. Dynamical methodsof soil and rock mechanics, Karlsruhe 1977, A. A. Balkema, Rotterdam, 1978, 2
10 Nelson, I. Constitutive models for use in numerical computations, Proc. Dynamical methods of soil and rock mechanics, Karlsruhe 1977, A. A. Balkema, Rotterdam, 1977, 2
11 Nelson, I. Two stage approach to dynamic soil structure interaction, K3/3, SMIRT 6, Paris, 1981
12 Waas, G. and Werkle, H. Response of nuclear power plant structures to the air pressure wave and the induced ground wave caused by gas explosions similar to detonations, part 2: induced ground wave, Hochtief AG, Abt. Kerntechnischer Ingenieurbau, Frankfurt, (1982, (in german)
13 Waas, G., Riggs, R. and Werkle, H. Displacement solutions for dynamic loads in a transversely-isotropic stratified medium, *Earthquake Engineering and Struct. Dynamics*, J. Wiley, Chichester, 1985
14 Waas, G. Analysis method for footing vibrations through layered media, Techn. Report S-71-14, No. 3, US Engineer Waterways Experiment Station, Vicksburg, Miss., 1972; also Linear two-dimensional analysis of soil dynamic problems in semi-infinite layered media, Dissertation, University of California, Berkeley, 1972
15 Kausel, E. An explicit solution for the Green functions for loads in layered media, MIT Research Report R81-13, 1981
16 Brigham, O. E. The fast Fourier transform, Prentice Hall Inc., Englewood Cliffs, New Jersey, 1974
17 Ewing, W. M., Jardetzky, W. S. and Press, F. Elastic waves in layered media, McGraw Hill, New York, 1957
18 Ferrieux, H. and Perrot, J. Effects telluriques des explosions de melanges hydrocarbures-air au dessus de la surface du sol, rapport SAER 81/29, CEA/DSN Fontenay-aux-roses, 1981

APPENDIX: ANALYSIS METHOD FOR GREEN'S FUNCTION

The equations of motion in a viscoelastic medium under plane strain conditions in frequency domain can be written:

$$\begin{bmatrix} (\lambda+2G)\dfrac{\partial^2}{\partial x^2}+G\dfrac{\partial^2}{\partial z^2}+\rho\omega^2 & (\lambda+G)\dfrac{\partial^2}{\partial x\partial z} \\ (\lambda+G)\dfrac{\partial^2}{\partial x\partial z} & (\lambda+2G)\dfrac{\partial^2}{\partial z^2}+G\dfrac{\partial^2}{\partial x^2}+\rho\omega^2 \end{bmatrix} \times \begin{Bmatrix} u \\ w \end{Bmatrix} = \underline{0} \qquad \text{(A1)}$$

with G being the complex shear modulus, λ the complex Lamé constant, ρ the mass density and ω the circular frequency of vibration. For a viscoelastic medium over a fixed base the boundary conditions are zero stress at the surface and zero displacements at the base.

A solution for the homogeneous equations (A1) is given by equation (2):

$$\begin{Bmatrix} u(x,z) \\ w(x,z) \end{Bmatrix} = \sum_j \alpha_j \cdot \begin{Bmatrix} X_j(z) \\ Z_j(z) \end{Bmatrix} \cdot e^{-i\cdot k_j x}$$

However the analytical solution for the functions $X_j(z)$ and $Z_j(z)$ leads to a nonalgebraic eigenvalues problem with complex eigenvalues k_j which is difficult to solve. Therefore the functions $X_j(z)$ and $Z_j(z)$ are approximated by shape functions with a linear variation in each layer, Fig. 1. The layer thickness must be chosen relatively thin in order that elastic waves are adequately represented by the assumed displacement functions (i.e., approximately 1/6 the length of a shear wave). Using a finite element approach, e.g., applying the principle of virtual displacements with the same shape functions for the virtual displacements $\hat{X}_j(z)$, $\hat{Z}_j(z)$ as for the actual displacement $X_j(z)$, $Z_j(z)$, an eigenvalue problem is obtained as:

$$(\underline{A}_R \cdot k_j^2 + \underline{B}_R \cdot k_j + \underline{C}_R) \cdot \begin{Bmatrix} \underline{X}_j \\ \underline{Z}_j \end{Bmatrix} = \underline{0} \qquad \text{(A2)}$$

The vector $\{\underline{X}_j\ \underline{Z}_j\}^T$ contains the values of the function $X_j(z)$. $Z_j(z)$ at the layer interfaces. The matrices $\underline{A}_R$, $\underline{B}_R$, $\underline{C}_R$ depend on the stiffness, damping and mass properties of the layers and are given in Ref. 13. The eigenvalues problem is algebraic and can be solved easily. It has $2 \cdot n_z$ generally complex wave numbers k_j and eigenvectors $\underline{X}_j$ and $\underline{Z}_j$, containing the horizontal and vertical displacement components, respectively. Only those eigenvalues, which correspond to waves, propagating away from the origin are selected. This leads to different solutions for $x>0$ and $x<0$.

The displacements, strains and stresses can now be expanded in terms of the eigensolutions. In order to compute the displacements caused by a line load at $x=0$, the domains $x \geqslant 0$ and $x \leqslant 0$ are considered. For both domains at $x=0$ the internal stresses and the external stresses (represented by the line loads) must be in equilibrium and displacements must be compatible. The fullfillment of these conditions leads to a solution for the Green's function. The displacements at a distance $x>0$ away from the line loads are

$$\begin{Bmatrix} \underline{u} \\ \underline{w} \end{Bmatrix} = \sum_{j=1}^{2n_z} \alpha_j \cdot \begin{Bmatrix} \underline{X}_j(z) \\ i\underline{Z}_j(z) \end{Bmatrix} \cdot e^{-ik_j x} \qquad \text{(A3)}$$

where $\underline{u}$, $\underline{w}$ are the horizontal and vertical displacements at the layer interfaces, respectively. The summation is performed over $2^* n_z$ modes, where n_z is the number of layers. The participation factors for a horizontal and a vertical line load acting at layer interface ζ are:

Vertical line load p_z:

$$\alpha_j = -\tfrac{1}{2} k_j \cdot Z_{\zeta j} \cdot p_z \qquad \text{(A4)}$$

Horizontal line load p_x:

$$\alpha_j = -\frac{i}{2} k_j \cdot X_{\zeta j} \cdot p_x \qquad \text{(A5)}$$

$X_{\zeta j}$ and $Z_{\zeta j}$ are the elements of the vectors $\underline{X}_j$ and $\underline{Z}_j$ at the layer interface ζ, respectively. The normalization of the eigenvectors is understood as in Refs 13 and 14. Details of the method are presented in Refs 12 to 15.